Molecular mechanism of gas diffusion in ice-Ih

Journal:	*ACS Earth and Space Chemistry*
Manuscript ID	sp-2021-00308n.R2
Manuscript Type:	Article
Date Submitted by the Author:	30-Sep-2021
Complete List of Authors:	Yi, Yoo Soo; Korea Polar Research Institute, Division of Glacial Environment Research Han, Yeongcheol; Korea Polar Research Institute, Kwon, Kideok; Kangwon National University, Geology Lee, Sung Keun; Seoul National University, School of Earth and Environmental Sciences Hur, Soon Do; Korea Polar Research Institute

Molecular mechanism of gas diffusion in ice-Ih

Yoo Soo Yi[*], **Yeongcheol Han**[*], **Kideok D. Kwon, Sung Keun Lee, and Soon Do Hur**

AUTHOR INFORMATION

Corresponding Author

Yoo Soo Yi – Division of Glacial Environment Research, Korea Polar Research Institute, Incheon 21990, Korea; orcid.org/0000-0002-5479-0357;
Email: yys2064@kopri.re.kr; yys2064@snu.ac.kr

Yeongcheol Han – Division of Glacial Environment Research, Korea Polar Research Institute, Incheon 21990, Korea; https://orcid.org/0000-0002-1729-7870;
Email: yhan@kopri.re.kr

Authors

Kideok D. Kwon – Department of Geology, Kangwon National University, Chuncheon 24341, Korea
Email: kkwon@kangwon.ac.kr

Sung Keun Lee – School of Earth and Environmental Sciences, Seoul National University, Seoul 08826, Korea
Email: sungklee@snu.ac.kr

Soon Do Hur – Division of Glacial Environment Research, Korea Polar Research Institute, Incheon 21990, Korea
Email: sdhur@kopri.re.kr

ABSTRACT

Atmospheric gases trapped in polar ice have been used to reconstruct polar and global climate changes, providing better time resolution when less diffused. Experiments have shown that gas diffusion in ice is negligible on a laboratory time scale, but its cumulative impact on old glacial ice (> 1 Myr) remains unclear. Here, we employ density functional theory calculations to investigate the diffusion mechanism of gases trapped in ice-Ih from the atomistic level. The results suggest that the diffusion energy barrier between interstitial sites is primarily dependent on the atomic size and charge distribution of hopping gases. The diffusion of noble gases (He, Ne, Ar, Kr, and Xe) primarily occurs via the interstitial mechanism, consistent with previous results of classical molecular dynamics simulations. In contrast, the precisely determined diffusion paths and energy barriers for CO_2, O_2, and N_2 suggest that these molecular gases prefer to hop along the hexagonal channel also via the interstitial mechanism, and the bond-breaking mechanism proposed previously to explain the diffusion of those molecular gases as fast as He and Ne may be unnecessary.

KEYWORDS

ice core, noble gases, gas diffusion mechanism, interstitial mechanism, paleorecord smoothing, density functional theory

INTRODUCTION

As an archive of climate records, polar ice cores, particularly the atmospheric gases preserved therein, have been used to reconstruct polar and global climate changes.[1-3] For instance, variations in CO_2 concentrations have reflected changes in the global carbon cycle and atmospheric temperature.[2, 4-5] The O_2/N_2 ratio has been used to estimate the atmospheric O_2 partial pressure relevant to changes in global erosion and ocean temperature.[6] This ratio is shown to have potential applications in orbital tuning of the ice core chronology, as it is affected by surface snow metamorphism associated with local summer insolation.[7-9] Additionally, isotope ratios of Ar ($^{\delta 40/38}$Ar and $^{\delta 38/36}$Ar) and Kr (^{81}Kr/Kr and ^{85}Kr/Kr) in trapped gases have been utilized for radiometric age dating of ice cores.[10-11]

The behavior of atmospheric air entrapped in accumulating ice sheets strongly depends on the porosity of the ice, which decreases with depth. While air resides within the interconnected porous structure of a firn column, ranging from near-surface snowpack down to the firn-ice transition depth (< 100 m), convective and diffusive gas mixing alters its gas composition over time.[12-14] Below the firn-ice transition depth, trapped air remains in the gas phase as air bubbles until it turns into air hydrates at bubble-clathrate transition depths below several hundred meters.[15-16] Mechanical mixing of gases is no longer allowed after bubble close-off, and gas permeation causing elemental and isotopic fractionation can only change the gas composition at a given depth. However, the gas dynamics in ice is much slower than gas mixing in the firn layer, and its effects have been considered minor. Indeed, experimentally determined diffusion rates of gases in ice are revealed to be negligible on a laboratory time scale.[17-20] For example, the displacement of Ar gas in ice would be less than $\sim 4\times10^{-4}$ m per hour, given its low diffusion coefficient (D) of $\sim 1.0\times10^{-11}$ $m^2\cdot s^{-1}$ (Table 1 for other gases) and the mean square displacement (MSD) of Ar $\leq 6Dt$ (where t is duration).[21]

Despite that, recent advances in deep ice core research give rise to the question of whether and how gas diffusion affects the paleorecords from old glacial ice, especially regarding the recent interest in glacial ice older than a million years.[5, 22-24] Based on a simple estimation using the experimentally determined D, the MSD of Ar in ice may reach up to the order of meters in 10 kyrs (MSD $\leq \sim 4.3$ m; Table 1). Diffusive gas exchange after close-off is mainly due to the gas permeation that usually occurs via the dissolution of gas at the bubble-ice interface (characterized by solubility, *S*) and then molecular diffusion through the ice (characterized by diffusivity, *D*).[16, 25-26] In most cases, the experimentally measured results correspond to the permeability (*P*) [17], which is the product of solubility and diffusivity ($S \times D$), but *S* and *D* are often required to be parameterized. For example, a numerical diffusive gas exchange model required *S* and *D*, and they were estimated indirectly by combining the experimental and theoretical results.[16] Another complication arises from the heterogeneity in glacial ices (e.g., ionic and structural defects, grain boundaries, and pore structures) that may serve as barriers to gas diffusion.[21, 27] In addition, the phase transition to the clathrate at greater depths would result in changes in the dynamics applied to the trapped gases because of the intrinsically distinct atomic structures of ice clathrate.[26, 28]

In understanding the complex phenomena of gas diffusion in glacial ice, theoretical studies have complemented experimental results. Previously, classical molecular dynamics (MD) simulations provided atomistic insight into the diffusion mechanism of various gases (He, Ne, Ar, N_2, O_2, CO_2, CH_4, and H_2O) in the ice-Ih lattice structure (Table 1).[29-31] These gases were shown to be trapped in two crystallographically distinct interstitial sites, namely, the uncapped trigonal (Tu) and capped trigonal (Tc) sites, and hop between them (see Figure 1). Diffusion-related parameters of those gases, such as *S* and *D*, were determined from the simulated diffusion trajectories at finite temperatures (< 270 K) using the Arrhenius-type diffusion equation. The results of classical MD simulations proposed that, while noble gases simply hop between adjacent interstitial sites (the interstitial mechanism), molecular gases (such as CO_2) tend to break the ice lattice structures along their hopping paths (the bond-breaking mechanism).[29-31] This bond-breaking mechanism is unusual for common crystals, but it was expected that relatively weak hydrogen bonds (H-bonds) would allow molecular gases to break the ice-Ih lattice structure during hopping.[29]

However, this atomistic description based on classical MD simulations needs to be revisited because of methodological limitations, particularly in describing complicated intermolecular interactions. To represent the intermolecular interactions, classical MD simulations applied empirical-parameter-based analytical potential functions to atoms/molecules assumed to have point/fixed charges (see Refs. for details of KKY interatomic potential model used in previous studies[29-32]).[33] Although corrections for the long-range dispersive forces such as H-bonds were made, the simplified intermolecular interactions may not properly account for the nonuniform molecular charge distributions of the hopping gases (i.e., characterized by the electrostatic potential surface). Furthermore, the differential electron density, estimated from the electron distribution, is important to determine the intermolecular interactions in ice (e.g., see Ref.[34] for the cooperative strengthening of local H-bonds in ice-Ih by neighboring H_2O molecules). In this regard, recently advanced theoretical methods that can precisely determine the intermolecular interactions from the total valence electron density distribution should be used to validate the gas diffusion mechanism in ice.

In this study, as a first step to comprehensive understanding of the gas permeation in polar ice cores occurring via *dissolution* at the gas-ice interface and *molecular diffusion* through the ice-Ih lattice structure, we investigate the diffusion mechanism of various gases dissolved in ice-Ih. Specifically, the diffusion paths and electronic diffusion energy barriers (E_D) of noble gases (He, Ne, Ar, Kr, and Xe) and other major atmospheric gases (CO_2, O_2, and N_2) are explored by employing DFT calculations. Recent advances in DFT calculations enable the accurate determination of intermolecular interactions between hopping gases and surrounding H_2O molecules from complete valence electronic structures.[35-36] Considerable differences from the previous classical MD simulation results, particularly for the diffusion mechanism of molecular gases and the relationship between E_D and the atomic sizes of the hopping gases, are presented. The conceptual advances achieved herein complement our understanding of the gas diffusion mechanism in glacial ice below the close-off depth, thereby stimulating further studies to probe precise diffusivity, dissolution processes (solubility), diffusion-assisted isotope fractionation, and numerical gas diffusion modeling for old glacial ice containing past atmospheric signals.

Table 1. Diffusion-related parameters of trapped gases in ice given in previous theoretical and experimental studies.

	[1] **Path**	[2] $\boldsymbol{D_0}$ ($m^2 \cdot s^{-1}$)	[2] $\boldsymbol{Q_{MD}}$ (eV)	[3] $\boldsymbol{D}$ ($m^2 \cdot s^{-1}$)	[3] $\boldsymbol{T}$ **(K)**	[4] **MSD (m)**
[5] **Theoretical results (classical MD simulations)**						
He	Tu-Tu$^{(V)}$	2.07×10^{-6}	0.17	8.25×10^{-10}	250	4.22×10^{-3}
	Tu-Tc-Tu$^{(H)}$	9.52×10^{-7}	0.18	2.66×10^{-10}	250	2.40×10^{-3}
	Average	1.63×10^{-6}	0.17	4.96×10^{-10}	250	3.27×10^{-3}
$\mathbf{N_2}$	Tu-Tu$^{(V)}$	7.41×10^{-11}	0.04	1×10^{-11}	250	4.65×10^{-4}
	Tu-Tc-Tu$^{(H)}$	8.05×10^{-10}	0.07	2.62×10^{-11}	250	7.52×10^{-4}
	Average	2×10^{-10}	0.05	1.74×10^{-11}	250	6.12×10^{-4}
$\mathbf{O_2}$	Tu-Tu$^{(V)}$	9.1×10^{-10}	0.09	1.38×10^{-11}	250	5.47×10^{-4}
	Tu-Tc-Tu$^{(H)}$	4.3×10^{-9}	0.09	5.94×10^{-11}	250	1.13×10^{-3}
	Average	3.5×10^{-9}	0.10	3.29×10^{-11}	250	8.43×10^{-4}
$\mathbf{CO_2}$	Tu-Tu$^{(V)}$	4.5×10^{-7}	0.20	5.06×10^{-11}	250	1.05×10^{-3}
	Tu-Tc-Tu$^{(H)}$	5.8×10^{-8}	0.14	1.06×10^{-10}	250	1.52×10^{-3}
	Average	9.1×10^{-8}	0.15	7.72×10^{-11}	250	1.29×10^{-3}
[5] **Experimental results**						
He	Tu-Tu$^{(V)}$	3.4×10^{-7}	0.12	1.30×10^{-9}	250	5.29×10^{-3}
	Tu-Tc-Tu$^{(H)}$	1.1×10^{-7}	0.13	2.63×10^{-10}	250	2.39×10^{-3}
He				1×10^{-9}–1.2×10^{-9}	258-268	4.65×10^{-3}–5.09×10^{-3}
Ne				6.2×10^{-11}–1.1×10^{-10}	258-268	1.16×10^{-3}–1.54×10^{-3}
Ar				~1×10^{-11}	258-268	4.65×10^{-4}

[1] Diffusion paths of hopping gases (see Figures 3a, 4a, and 5a).
[2] Preexponential factors (D_0) and dynamic diffusion energy barriers (Q_{MD}) determined from classical MD simulations[29-31] and experiments[17-19] by applying the Arrhenius-type equation to the simulated diffusion trajectory.
[3] Diffusion coefficients (D) at a given temperature (T) estimated as per the Arrhenius-type diffusion equation with corresponding D_0 and Q_{MD}.
[4] Mean squared displacements (MSD) per hour when D is given and normal diffusion is assumed, i.e., $(6Dt)^{1/2}$. The actual MSD would be less due to hindrance by the lattice structure and structural heterogeneities, including defects, grain boundaries, and pore structures.[21]
[5] Diffusion-related parameters for He,[31] H_2O,[31] N_2,[30] O_2,[29] CH_4,[29] and CO_2[29] obtained by the classical MD simulations and those for H_2O,[18] H_2,[19] He,[17, 20] Ne,[17] and Ar[17] determined experimentally.

METHODS

Ice-Ih with extrinsic gases

The ice-Ih structure used to investigate the gas diffusion mechanism was retrieved from previous X-ray diffraction data.[37] Natural ice usually contains diverse structural and ionic defects due to molecular disorientation and vacancies (e.g., Bjerrum defects).[38-39] In this study, however, the fully ordered and defect-free ice-Ih structure was chosen to simplify the diffusion model and improve the efficiency of calculations. The supercell structure, consisting of 144 H_2O molecules with lattice parameters of 13.5480 Å, 15.6439 Å, and 21.8123 Å for the *a*-, *b*-, and *c*-axes, was used to reduce the interactions originating from the periodically repeated images (e.g., interaction between the repeated extrinsic gases). The hopping paths of the extrinsic gases were determined from the topological arrangements of the Tu and Tc sites illustrated in Figure 1: (1) Tu-Tu$^{(V)}$ (hopping from Tu to Tu through the open hexagonal channel parallel to the *c*-axis) and (2) Tu-Tc-Tu$^{(H)}$ or Tu-Tu$^{(H)}$ (hopping from Tu to Tu between the horizontally stacked bilayers in the *ab*-plane either passing through or bypassing the center of the adjacent Tc site). Throughout the manuscript, the superscripts (V) and (H) indicate either the direction of the hopping path or the molecular orientation (vertical along the *c*-axis and horizontal in the *ab*-plane).

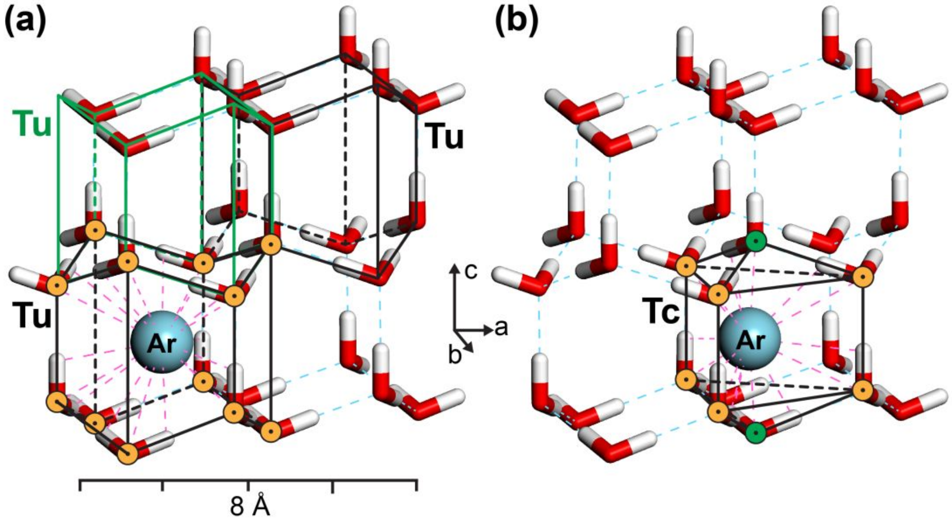

Figure 1. Crystallographically distinct interstitial sites in the ice-Ih lattice structure (trapped Ar atoms are shown as examples). **(a)** The uncapped trigonal site (Tu). It is surrounded by 12 H_2O molecules (orange circles) and is part of an open hexagonal channel parallel to the *c*-axis. **(b)** The capped trigonal site (Tc). It is surrounded by 6 H_2O molecules (orange circles) and capped with two H_2O molecules (green circles).

Calculations

DFT calculations have been used to investigate various materials necessary for environmental and solid earth studies, e.g., the chemical reactions at interfaces[40-44] and the atomic and electronic structures under extremely high pressures[45-51]. The calculation parameters used here were determined and adjusted based on these previous studies. Electronic structure calculations, geometry optimizations, and transition state searching (TSS) were carried out using CASTEP.[35] The interatomic interactions were described with the on-the-fly generation ultrasoft pseudopotential and the Perdew-Burke-Ernzerhof (PBE) exchange-correlation functional.[35, 52] The plane-wave cutoff energy of 800 eV, the convergence criterion for self-consistent-field (SCF) calculations of 1×10^{-6} eV·atom^{-1}, and the Monkhorst-Pack (MP) grid for Brillouin zone sampling of 1×1×1 (i.e., Γ point) were applied. The long-range dispersion intermolecular interactions, which are indispensable for molecular crystals,[36, 51] were corrected with the Tkatchenko–Scheffler (TS) method.[53] In addition, the scalar relativistic correction via the Koelling-Harmon method was applied consistently in all calculations to improve the accuracy of the calculations, including relatively heavy elements (i.e., Kr and Xe).[54] Geometry optimization to determine the most stable configurations of ice-Ih containing extrinsic gases was carried out through the two-point steepest descent (TPSD) algorithm with convergence criteria of 1×10^{-5} eV·atom^{-1}, 0.03 eV·Å^{-1}, 0.05 GPa, and 0.001 Å for the total energy, maximum force, maximum stress, and maximum displacement, respectively.[55] The diffusion paths of hopping gases and the corresponding energy changes, as well as the electronic diffusion energy barrier (E_D), were precisely determined via TSS calculations, which were carried out via the synchronous transit method (LST/QST) with a convergence criterion of 0.05 eV·Å^{-1}.[56]

The convergence of the total energy was tested by varying the cutoff energy (600–1400 eV), the SCF tolerance (2×10^{-6}–5×10^{-7} eV·atom^{-1}), and the MP grid (1×1×1–3×3×3); the results sufficiently converged with the parameters listed above. The convergence of E_D was also examined for He, Ar, and Kr gases by comparing the results with those obtained by employing more accurate parameters (5×10^{-6} eV·atom^{-1}, 0.01 eV·Å^{-1}, 0.02 GPa, and 5×10^{-4} Å for geometry optimizations and 0.01 eV·Å^{-1} for TSS); the results converged within the order of ~0.01 eV, but the deviation increased slightly with increasing atomic size of the hopping gas. The calculated total energies and E_D for relatively large noble gases and molecular gases also differed slightly even at crystallographically identical sites or paths. This might be due to the structural instability of the finite-sized ice-Ih supercell structure containing extrinsic gases. Nevertheless, given the above discussed validation of total energy and E_D, the accuracy of the results was sufficient to address the diffusion mechanism of gases trapped in ice-Ih. A previous study showed that PBE-TS calculations could provide comparable results to those of highly accurate calculations, e.g., the post-Hartree-Fock method and the hybrid functional of PBE and the Hartree-Fock exchange terms (i.e., PBE0) with TS dispersion correction (PBE0-TS). However, intermolecular interactions, such as hydrogen bonds between H_2O molecules, could be slightly overestimated.[36]

To compare and verify inaccuracies in classical MD simulations, we calculated the potential energy profiles of CO_2/ice-Ih between adjacent Tu sites along the *c*-axis using 2nd-order Moller–Plesset (MP2) perturbation theory. The MP2 method is a wave-function-based method that is often used to validate DFT results for van der Waals (vdW) or hydrogen bond (H-bond) dominant systems.[57] The MP2 calculations were carried out using a CO_2/ice-Ih cluster model containing 18 H_2O molecules with three different sizes of the basis set, i.e., STO-3G, 6-31G(d), and aug-cc-pVDZ, in Gaussian 09.[58]

Diffusion dynamics are usually described by the Arrhenius-type diffusion equation [$D = D_0 \cdot \exp(-E_D/k_B T)$]. We could determine the E_D values for gases hopping in the ice-Ih lattice. However, determining the pre-exponential factor (D_0) further requires phonon calculations, as it indicates the ratio between the products of vibration modes for the initial and transition states of gas diffusion (i.e., the so-called attempt frequency; $v_0 \approx \Pi_i^N v_i / \Pi_j^{N-1} v_j$ for the vibrational modes at the initial state, *i*, and transition state, *j*; see details in Ref.[59]). Given the definition of attempt frequency (v_0), its value for each hopping path may present a nonnegligible difference. Despite that, we assumed almost identical v_0 for each path (i.e., $v_0^{(V)} \approx v_0^{(H)}$) to estimate the diffusion energy barrier for the total diffusion flux (i.e., the apparent diffusion energy barrier, $\langle E_D \rangle$). Here, $\langle E_D \rangle$ was determined as follows:

$$\langle E_\mathrm{D} \rangle \approx -k_\mathrm{B}T \cdot \ln \left[\exp\left(-\frac{E_\mathrm{D}^{(\mathrm{V})}}{k_\mathrm{B}T} \right) + \exp\left(-\frac{E_\mathrm{D}^{(\mathrm{H})}}{k_\mathrm{B}T} \right) \right]$$

$E_\mathrm{D}^{(\mathrm{V})}$ and $E_\mathrm{D}^{(\mathrm{H})}$ refer to the electronic diffusion energy barriers for the hopping gases along the vertical and horizontal paths, respectively. This semiquantitative analysis is expected to be helpful for understanding the trend of diffusion flux.

RESULTS AND DISCUSSION

DFT and classical MD simulations

The DFT calculations showed significantly different results from previous MD simulations with respect to molecular orientation, stable sites, and diffusion mechanism. For instance, classical MD simulations relying on empirical potentials identified the Tu site as a stable site for CO_2 binding.[29] However, in this study, CO_2 tended to be rather stable between two adjacent Tu sites. Figure 2 demonstrates that as the basis set size increased, the energy minimum was closer to the DFT-calculated E_D value. The MP2 calculations with a large basis set, aug-cc-pVDZ, also predicted the energy minimum between Tu sites in line with the current DFT calculation. The trend of the previous MD simulations, showing the energy minimum at the Tu site, was only reproducible with STO-3G, the minimal basis set whose accuracy was much inferior to that of the other basis sets. These results validate our DFT calculation results but indicate the inaccuracy of the empirical-parameter-based force field calculations.

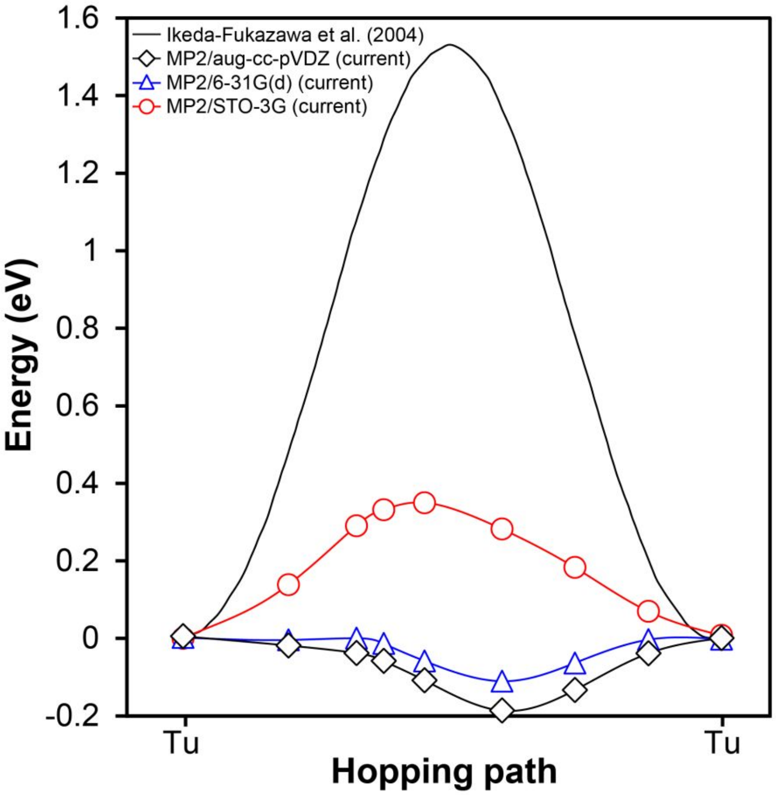

Figure 2. Electrostatic potential barriers acting on the CO_2 molecule hopping through the open hexagonal channel parallel to the *c*-axis (Figure 4a) calculated here at the MP2 level perturbation theory with different sizes of basis sets; STO-3G (red line with circles), 6-32G(d) (blue line with triangles), and aug-cc-pVDZ (black line with diamonds). Data of the previous MD study was from Ikeda-Fukazawa et al., 2004 (black solid line).[29]

Diffusion of noble gases

Figure 3 presents the diffusion paths and corresponding energy changes (ΔE) of noble gases (He, Ne, Ar, Kr, and Xe) trapped in ice-Ih. On the Tu-Tu$^{(V)}$, Tu-Tc-Tu$^{(H)}$, and Tu-Tu$^{(H)}$ hopping paths, transition states were found at the boundaries between adjacent interstitial sites with slight shifts of H_2O molecules (Figure 3a). In Figure 3b, the ΔE values of the hopping gases, equivalent to the energy required to hop between adjacent interstitial sites (E_D), are presented for different diffusion coordinates. Whereas the largest atoms, Xe, did not prefer to be trapped inside the relatively small H_2O molecule-capped Tc sites, He, Ne, Ar, and Kr atoms could be trapped therein. The total energy of ice/gas increased significantly after hopping to the Tc site due to the distortions of nearby lattice structures: ~0.18 eV for He, ~0.34 eV for Ne, ~0.69 eV for Ar, and ~0.84 eV for Kr (Figure 3b). Then, the proportion of noble gases trapped in the Tc site would be exceedingly small because the larger the energy differences are the greater the preference of the Tu site. The ΔE at the Tc site and the E_D for all available paths increase with increasing atomic sizes of the hopping gases. This result agrees with the physical intuition that larger atoms require greater energy to pass the boundary between adjacent interstitials, as they need greater structural distortion. The atomic-size dependence of E_D will be further discussed together with the results of molecular gases in Figure 7.

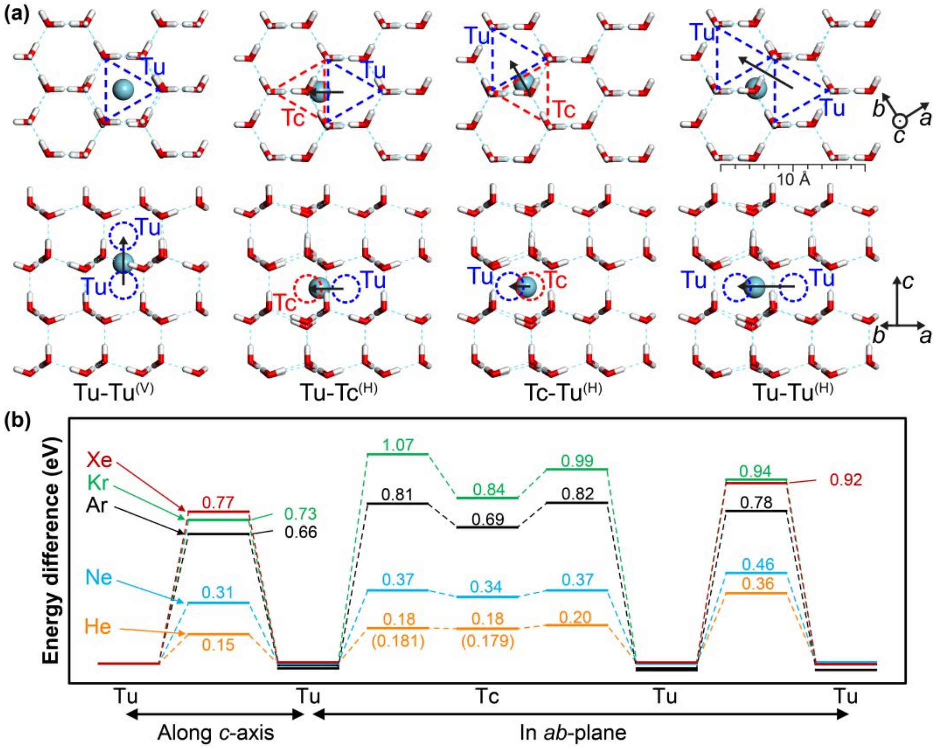

Figure 3. (a) Diffusion paths of noble gases (He, Ne, Ar, Kr, and Xe) trapped in ice-Ih, along the vertically aligned open hexagonal channel parallel to the *c*-axis (V) and between the horizontally stacked bilayers in the *ab*-plane (H): Tu-Tu$^{(V)}$, Tu-Tc-Tu$^{(H)}$ (hopping along Tu-Tc$^{(H)}$ and then Tc-Tu$^{(H)}$), and Tu-Tu$^{(H)}$. The transition states of each hopping process are

presented. **(b)** Energy differences (ΔE) of the hopping gases for different diffusion coordinates and electronic diffusion energy barriers (E_D) given relative to the energy at the most stable Tu site.

Diffusion of molecular gases

Compared to noble gases, CO_2, O_2, and N_2 gave more complicated results depending on their orientations, sizes, and charge characteristics. Figure 4 presents the energy changes of vertically oriented CO_2, O_2, and N_2 gases hopping along the Tu-Tu$^{(V)}$ path (i.e., the open hexagonal channel parallel to the *c*-axis). The O_2 and N_2 gases were stable when they were entirely trapped in the Tu site, and their transition states were reached at the boundary between the vertically aligned Tu sites (Tu···Tu; see Figure 4a). The E_D of N_2 hopping along the Tu-Tu$^{(V)}$ path, i.e., $E_D^{(V)}(N_2)$, was larger than $E_D^{(V)}(O_2)$ by ~0.15 eV despite the similar atomic sizes of N and O (the vdW radii, R_W, of N and O atoms are ~155 pm and ~152 pm, respectively). This result could be attributed to the distinctly different charge distributions of N_2 and O_2 molecules. O_2 exhibits almost homogeneous and neutral charge character, but N_2 has a significant gradient in the molecular charge distribution ($^{[-]}N^{[+]}N^{[-]}$) due to the presence of lone-pair electrons and hence induces stronger intermolecular interactions with nearby H_2O molecules on the hopping paths.[60] In contrast to O_2 and N_2 molecules, CO_2 was stabilized when it was hanging at the open hexagonal ring in a perpendicular direction with its carbon atom at the center (at Tu···Tu; Figure 4a); the ΔE at Tu···Tu was lower by ~0.2 eV (see Figure 4b). This result, different from those of N_2 and O_2, might be primarily due to the strong intermolecular interactions between CO_2 and neighboring H_2O molecules, as shown in Figure 4a: the interactions between positively charged C ($^{[+]}C$) of the CO_2 molecule and negatively charged oxygen ($^{[-]}O$) of surrounding H_2O molecules in the hexagonal ring and between $^{[-]}O$ of the CO_2 molecule and $^{[+]}H$ of nearby H_2O molecules. Furthermore, CO_2, even with the relatively large carbon atom (~170 pm of R_W), had a smaller $E_D^{(V)}(CO_2)$ than those for N_2 and O_2: $E_D^{(V)}(N_2) > E_D^{(V)}(O_2) > E_D^{(V)}(CO_2)$. It can then be concluded that, for the diffusion of CO_2, the characteristic charge distribution was more influential than its size. In addition, the energy required for the structural distortion of the ice-Ih lattice structure by slightly pushing aside H_2O molecules on the hopping path would be included in E_D for these molecular gases; see below the effect of lattice distortion on the E_D of CO_2 (Figure 5).

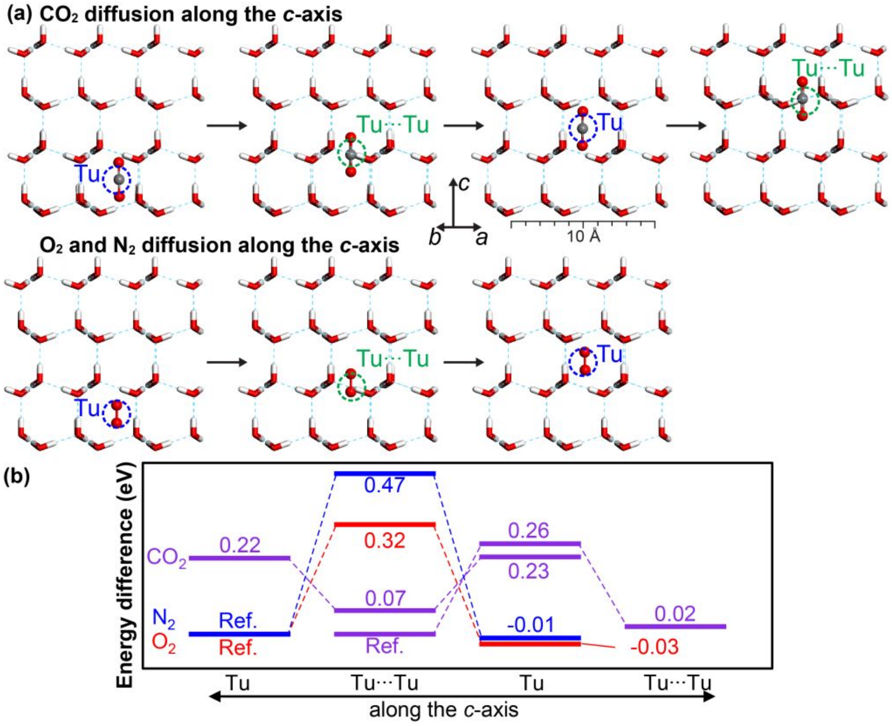

Figure 4. (a) Diffusion paths of vertically oriented molecular gases (CO_2, O_2, and N_2) trapped in ice-Ih along the Tu-Tu$^{(V)}$ path (the open hexagonal channel parallel to the *c*-axis). The initial, transition, and final states are presented. **(b)** Energy differences (ΔE) of the hopping gases for the diffusion coordinates and electronic diffusion energy barriers (E_D) compared to the energy at the most stable site.

Figure 5 presents the diffusion paths and corresponding energy changes of horizontally oriented CO_2, O_2, and N_2 gases hopping along the Tu-Tu$^{(H)}$ path between the horizontally stacked bilayers. As shown in Figure 5a, horizontally oriented linear molecular gases tended to bypass the center of the Tc site. Figure 5b shows that the calculated E_D for these horizontally oriented molecular gases, $E_D^{(H)}$, was higher than the corresponding $E_D^{(V)}$, but the trend was similar: $E_D^{(H)}(N_2) > E_D^{(H)}(O_2) > E_D^{(H)}(CO_2)$. Both O_2 and N_2 molecules could be entirely trapped in the Tu site even when horizontally oriented. Thus, the difference between $E_D^{(H)}(N_2)$ and $E_D^{(H)}(O_2)$ might be due to their distinct molecular charge distributions, as discussed above. In contrast, the longer CO_2 molecule was not entirely trapped in the Tu site (Figure 5a); one of the oxygen atoms was likely to be in the Tc site. In addition to the characteristic molecular charge distribution, this stable configuration of CO_2 across the boundary between adjacent Tu sites would affect $E_D^{(H)}(CO_2)$. It already deforms the relatively small Tc site by pushing aside H_2O molecules and, thus, may decrease the energy required for the structural distortion that facilitates CO_2 hopping.

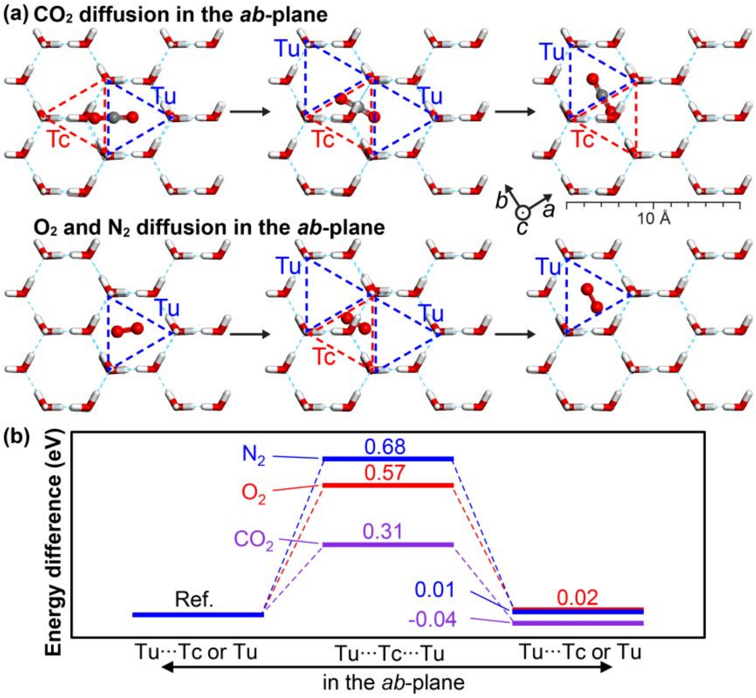

Figure 5. (a) Diffusion paths of horizontally oriented molecular gases (CO_2, O_2, and N_2) trapped in ice-Ih along the Tu-Tu$^{(H)}$ path (between the horizontally stacked bilayers in the *ab*-plane). The initial, transition, and final states of each hopping are presented. **(b)** Energy differences (ΔE) of the hopping gases for the diffusion coordinates and electronic diffusion energy barriers (E_D) compared to the energy at the most stable site.

In addition to the molecular orientation-specific diffusion of CO_2, O_2, and N_2 molecules, Figure 6 presents the energy required to change their molecular orientations in the ice-Ih lattice (E_R). As shown in Figure 6a, the relatively small O_2 and N_2 molecules (molecular lengths of ~1.22 Å and ~1.10 Å, respectively) can rotate even when they are trapped in the Tu site. The stronger intermolecular interaction of N_2-H_2O than of O_2-H_2O, induced from the characteristic charge distributions of N_2,[60] led to $E_R(N_2) > E_R(O_2)$, as shown in Figures 4 and 5. In contrast, the CO_2 molecule (with a longer molecular length of ~2.34 Å) should pivot around the adjacent Tc center to change its molecular orientation. Thus, the $E_R(CO_2)$ was greater than those of N_2 and O_2: $E_R(CO_2) > E_R(N_2) > E_R(O_2)$. In addition, we found that the total energy of ice/gas increases after rotation of the molecular gases from vertical to horizontal by ~0.22 eV for CO_2, ~0.10 eV for N_2, and ~0.08 eV for O_2 (Figure 6b), implying relative instability compared to vertically oriented molecules. Then, the proportion of vertically oriented molecules would be greater than that of horizontally oriented molecules; the lower the total energy is, the more likely the configuration is to exist.

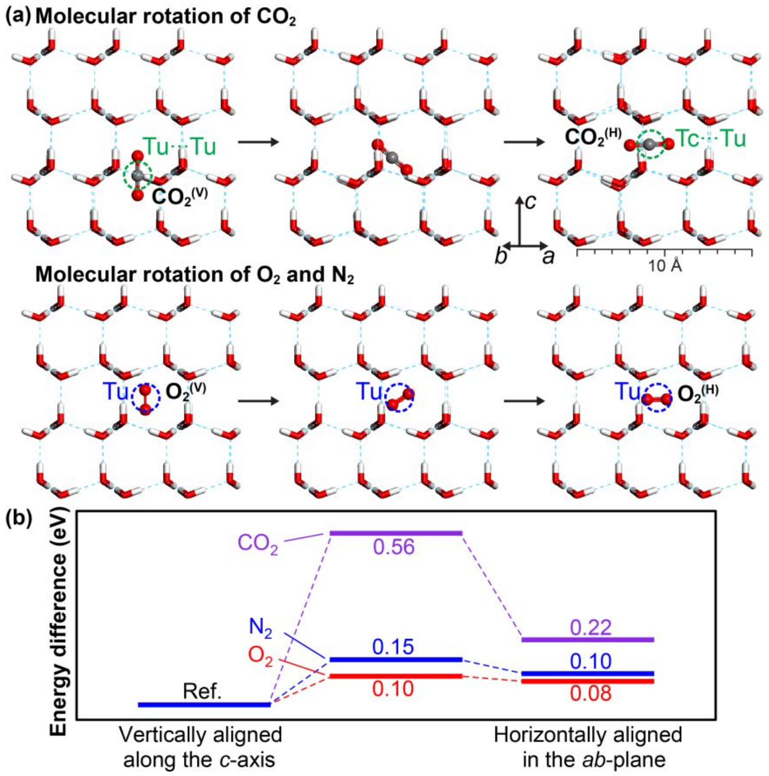

Figure 6. (a) Molecular rotations of molecular gases (CO_2, O_2, and N_2) trapped in ice-Ih, from the vertical direction (parallel to the *c*-axis) to the horizontal direction (in the *ab*-plane). The initial, transition, and final states of each hopping are presented. **(b)** Energy differences (ΔE) of the rotating gas molecules and electronic rotation energy barriers (E_R) compared to the energy at the most stable states.

Gas diffusion mechanism

A systematic understanding of the tendency of gas diffusion in ice-Ih is possible by combining the results in Figures 3–6. Figure 7a presents the relationship between E_D and R_W of the largest atom of the hopping gases. Previous classical MD simulations reported that the molecular diffusion of CO_2, O_2, and N_2 trapped in ice-Ih is easier between the stacked bilayers in the *ab*-plane than along the *c*-axis.[29] In contrast, the current results, showing the lowest E_D for the Tu-Tu$^{(V)}$ path, demonstrate that molecular diffusion through the open hexagonal channel parallel to the *c*-axis is the primary mechanism for both noble and molecular gases rather than the other horizontal paths between the stacked bilayers in the *ab*-plane. For hopping in the *ab*-plane, the trendlines of Tu-Tc$^{(H)}$ and Tu-Tu$^{(H)}$ imply that (1) He and Ne preferred the Tu-Tc-Tu$^{(H)}$ path passing through the center of the adjacent Tc site but (2) relatively large Ar, Kr, and Xe preferred the Tu-Tu$^{(H)}$ path that bypasses the center of the adjacent Tc site. Note that the E_D of Tc-Tu$^{(H)}$ indicates additional energy for the subsequent hopping from the intermediate state (Tc) to the final state (Tu) in the Tu-Tc-Tu$^{(H)}$ path.

Together with the site- and orientation-specific stability and preference of the gases trapped in ice-Ih (see Figure 1 for noble gases and Figure 6 for CO_2, O_2, and N_2), this refined perspective could improve the mechanistic and atomistic understanding of the experimentally measured diffusion-related phenomena, or those cannot be measured yet. For instance, a previous study reported that the randomized *c*-axis distribution of ice particles (characterized by the lattice preferred orientation) at the upper region tends to converge in the vertical direction of the glacier with depth because the dominance of deformation modes changes from vertical compression in the upper part to horizontal shear in the lower part (see Ref.[61] for details). In this circumstance, the preferred gas diffusion through the open hexagonal channel parallel to the *c*-axis suggests anisotropic gas diffusion in deep glaciers along the vertical direction, as assumed in the previous numerical models.[16, 26]

Figure 7b shows the apparent diffusion energy barrier, $\langle E_D \rangle$, for the total flux of gas diffusion in ice-Ih (see Methods for details). The $\langle E_D \rangle$ of hopping gases, which appeared to be primarily determined from the E_D of the most preferred Tu-Tu$^{(V)}$ path, increases with increasing R_W: $\langle E_D \rangle \approx 0.01 \times R_W - 0.92$ ($R^2 = 0.83$). We noted that the $\langle E_D \rangle$ of CO_2 and N_2 notably deviates from the overall trend. Figure 7c shows the relative diffusivity (D/D_0) of gases hopping via the interstitial mechanism. These values are estimated from the $\langle E_D \rangle$ as per the Arrhenius-type diffusion equation, i.e., $\exp[-\langle E_D \rangle / k_B T]$, and quantification of the absolute diffusion rate (D) further requires the pre-exponential factor (D_0) to be determined. Details will be discussed in the Further studies section. Considering the nonuniform charge distributions of CO_2 and N_2 molecules, this result suggests that the diffusion dynamics in ice are determined primarily by the sizes of hopping gases, but the charge characteristics of hopping gases also affect it. Note that the relationship between $\langle E_{\mathrm{D}} \rangle$ and R_{W} may differ from this simple linear pattern together with the results of larger-sized and/or distinctively charged molecular gases in future studies.

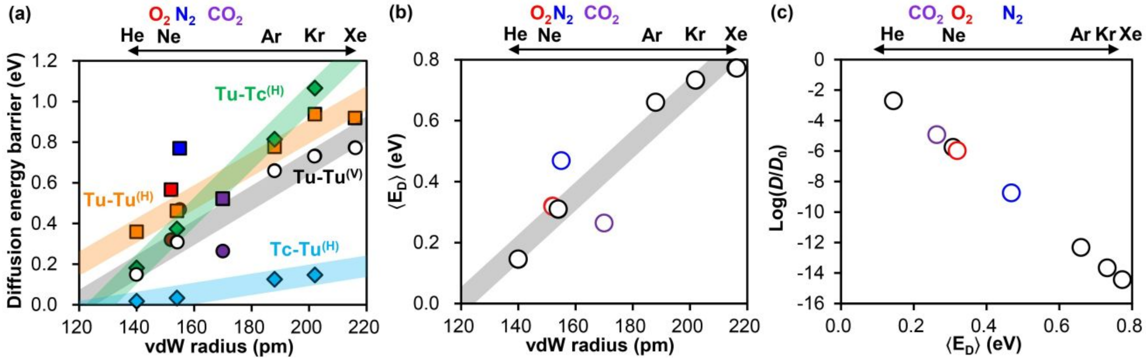

Figure 7. (a) Relationships between the electronic energy barriers (E_{D}) and the van der Waals radii (R_{W}) of the hopping gases trapped in ice-Ih for each path: Tu-Tu$^{(\mathrm{V})}$ (white circles), Tu-Tu$^{(\mathrm{H})}$ (orange squares), Tu-Tc$^{(\mathrm{H})}$ (green diamonds), and Tc-Tu$^{(\mathrm{H})}$ (cyan diamonds). The solid lines indicate the E_{D} trends of noble gases only. The results for CO_2 (purple), O_2 (red), and N_2 (blue) are presented for the Tu-Tu$^{(\mathrm{V})}$ (circles) and Tu-Tu$^{(\mathrm{H})}$ (squares) paths. **(b)** Relationship between the apparent diffusion energy barrier, $\langle E_{\mathrm{D}} \rangle$, and R_{W} for the whole data set: $\langle E_{\mathrm{D}} \rangle \approx 0.01 \times R_{\mathrm{W}} - 0.92$ ($R^2 = 0.83$). **(c)** Semi-quantitatively predicted relative diffusivity (D/D_0) of the gases hopping via the interstitial mechanism (Figures 3, 4, and 5); $D/D_0 = \exp[-\langle E_{\mathrm{D}} \rangle / k_{\mathrm{B}}T]$ at 270 K.

The energy barriers along the diffusion paths for He, Ne, Ar, N_2, O_2, and CO_2 determined here and in previous studies[29-31] are summarized in Table 2 to compare the tendency of gas diffusion dynamics: the electronic diffusion energy barrier (E_{D}) determined via DFT calculations (Figure 7), the potential barrier (E_{MD}) acting on the hopping gases, and the diffusion coefficients (D_{MD}) retrieved from classical MD simulations. In the following discussion, E_{D} and E_{MD}, D_{MD}, indicate $\langle E_{\mathrm{D}} \rangle$, $\langle E_{\mathrm{MD}} \rangle$, and $\langle D_{\mathrm{MD}} \rangle$, respectively (see Methods).

Previous classical MD simulations determined the relative differences in the potential barriers acting on the hopping gases (E_{MD}) in ice-Ih (Table 2): $E_{MD}(He) < E_{MD}(Ne) < E_{MD}(Ar) < E_{MD}(O_2) < E_{MD}(N_2) < E_{MD}(CO_2)$. The E_{MD} increased with the atomic/molecular size of the hopping gases. If interstitial hopping prevails, the E_{MD} should be inversely correlated with the diffusion coefficient (D_{MD}) as per the Arrhenius-type diffusion equation. However, the diffusion of molecular gases was revealed to be faster than the interstitial mechanism could explain, and thus, the order of D_{MD} dramatically differed from that predicted from E_{MD} assuming interstitial hopping: $D_{MD}(He) > D_{MD}(CO_2) > D_{MD}(Ne) > D_{MD}(O_2) > D_{MD}(Ar) > D_{MD}(N_2)$. The previous study suggested that this difference is a consequence of the anomalous bond-breaking mechanism (i.e., occurred by breaking the ice lattice structure along the hopping path).

Compared to the previous classical MD results,[29] the DFT calculations showed significant differences in the potential barrier acting on the hopping gases and the gas diffusion mechanism, particularly for CO_2, O_2, and N_2 gases. The results of noble gases (He, Ne, and Ar) show that interstitial hopping is predominant, as previously suggested. In addition, we found that CO_2, O_2, and N_2 gases also tend to hop along the open hexagonal channel via the interstitial mechanism instead of the previously suggested bond-breaking mechanism (Figures 4, 6, and 7a). The calculated E_D values for these molecular gases were surprisingly small and rather comparable to He and Ne than the other large atomic gases. Consequently, the order of E_D is significantly different from E_{MD}: $E_D(He) < E_D(CO_2) < E_D(Ne) < E_D(O_2) < E_D(N_2) < E_D(Ar) < E_D(Kr) < E_D(Xe)$ (see Table 2 and Ref.[29]). In principle, the E_D and E_{MD} trends should be similar or identical because they both originate from intermolecular interactions between the hopping gases and the surrounding H_2O molecules; however, the difference is substantial, as shown in Table 2. We ascribed these discrepancies to the methodological limitations of classical MD simulations in describing the intermolecular interactions (Figure 2). We noted noticeable differences between E_D and E_{MD} (e.g., $E_D > E_{MD}$ for noble gases and $E_D < E_{MD}$ for CO_2, O_2, and N_2), but the direct comparison is not straightforward because they were obtained from completely different theoretical methods.

Since E_D governs the diffusion dynamics as per the Arrhenius equation (via the interstitial mechanism), the diffusivity (D_{DFT}) might be inversely correlated with E_D within a typical temperature range of experiments or the cryosphere (below the melting point). Then, the order of gas diffusivity would be $D_{\mathrm{DFT}}(\mathrm{He}) > D_{\mathrm{DFT}}(\mathrm{CO_2}) > D_{\mathrm{DFT}}(\mathrm{Ne}) > D_{\mathrm{DFT}}(\mathrm{O_2}) > D_{\mathrm{DFT}}(\mathrm{N_2}) > D_{\mathrm{DFT}}(\mathrm{Ar}) > D_{\mathrm{DFT}}(\mathrm{Kr}) > D_{\mathrm{DFT}}(\mathrm{Xe})$ (see Figure 7c). This result demonstrates that the fast diffusion of molecular gases (CO_2, O_2 and N_2) can arise from the interstitial hopping mechanism instead of the bond breaking mechanism suggested in previous studies using classical MD simulations.[29-31] Note that the order of gas permeability can differ depending on the solubility of gases at the gas-ice interface (see the Further studies section for details).

Table 2. Diffusion energy barriers of hopping gases trapped in ice determined in this study (E_D; eV) and in previous classical MD studies (E_{MD}; eV).

	^{1} **Tu-Tu$^{(V)}$**		^{1} **Tu-Tc-Tu$^{(H)}$ or Tu-Tu$^{(H)}$**		^{2} **Apparent diffusion**	
	^{3} $E_D^{(V)}$	^{4} $E_{MD}^{(V)}$	^{3} $E_D^{(H)}$	^{4} $E_{MD}^{(H)}$	$^5\langle E_D \rangle$	$^6\langle E_{MD} \rangle$
CO_2	0.26	1.53	0.52	8.27	0.26	~1.53
O_2	0.32	0.42	0.57	2.31	0.32	~0.42
N_2	0.47	0.48	0.77	2.67	0.47	~0.48
Ar	0.66	0.28	0.78	1.54	0.66	~0.28
Ne	0.31	0.07	0.37	0.36	0.31	~0.07
He	0.15	0.03	0.18	0.12	0.14	~0.03

[1] Diffusion paths of hopping gases (Figures 3a, 4a, and 5a).

[2] Diffusion energy barriers estimated for the apparent diffusion, indicating the trend of total diffusion flux: $\langle D \rangle = D^{(V)} + D^{(H)}$.

[3] Electronic diffusion energy barriers (E_D) acting on the vertically ($E_D^{(V)}$) and horizontal ($E_D^{(H)}$) hopping gases calculated herein using DFT calculations (Figure 7).

[4] Potential barriers (E_{MD}) acting on the hopping gases estimated with the analytical potential functions used in the classical MD simulations.[29-31]

[5] Apparent diffusion energy barrier, $\langle E_D \rangle$, determined from the directional-specific energy values. See details in the Methods.

[6] Apparent diffusion energy barrier, $\langle E_{MD} \rangle$, and diffusion coefficients, $\langle D_{MD} \rangle$, retrieved from the previous classical MD study.[29]

Further studies

The current results suggest that interstitial hopping is the primary diffusion mechanism for noble and molecular gases trapped in ice-Ih. Thus, we could present the relative diffusivity of gases based on the calculated diffusion energy barrier (E_D) acting on the hopping gases as per the Arrhenius-type diffusion equation. Nevertheless, to quantitatively estimate the hopping probability and diffusion rate, the pre-exponential factor (D_0) of the Arrhenius-type diffusion equation needs to be determined from the attempt frequency (ν_0) of gas diffusion and the structural factors (e.g., the number of hopping sites, the hopping distance, and the dimension of diffusion). The attempt frequency can be calculated from the changes in vibration modes of the gas atom/molecule and the surrounding H_2O molecules during the hopping process ($\nu_0 = \prod_i^N \nu_i / \prod_j^{N-1} \nu_j$, where ν_i and ν_j refer to the total vibration modes at the initial and transition states respectively; see Ref.[59] for details). If the attempt frequency of gas diffusion is quantitatively determined, it can be applied to the investigation of diffusion-assisted isotope fractionation in old glacial ices. In addition to the current results for CO_2, O_2, and N_2 gases, the diffusion mechanism of CH_4, one of the prominent greenhouse gases, needs to be further explored because of its substantially different molecular geometry.

As discussed above, ice core paleorecord smoothing after close-off is generally attributed to gas permeation from one bubble to another through the ice layer, which can be understood as a two-step process: (i) gas dissolution at the gas-ice interface via adsorption on the ice surface and penetration into the ice lattice structure and (ii) molecular diffusion through the ice-Ih lattice structure.[16, 25-26] Since this study has focused on the molecular diffusion mechanism, the gas dissolution process (i.e., solubility) needs to be further explored to fully understand the gas permeation in ice (e.g., see Ref. for the CO_2 diffusion model, considering both solubility and diffusivity[4]). Figures 3 and 6 show the positive relationship between the structural instability of gas/ice system and the size of hopping gases, which may suggest that the solubility (S) also has the trends of $S(\mathrm{He}) > S(\mathrm{Ne}) > S(\mathrm{Ar}) > S(\mathrm{Kr}) > S(\mathrm{Xe})$ for the noble gases and $S(O_2) > S(N_2) > S(CO_2)$ for the molecular gases. However, their overall trend can be different from that of diffusivity expected from E_D, since the molecular gases (e.g., CO_2 and N_2) can have very low solubility due to their molecular geometries and characteristic electrostatic charge distribution. For example, the CO_2 molecule has negative partial charges at both ends and can be strongly adsorbed to the unpaired H atoms on the ice surface (see Ref. for the CO_2 adsorption model on ice surface[62]), requiring large energy to penetrate the ice lattice structure by overcoming the strong bindings with surface protons (i.e., corresponding to the activation energy for dissolution; E_S). Then, its solubility can be extremely low, which would not be case for the noble gases. Consequently, the trend of permeability ($P = S \times D$) would be different from that of diffusivity established in this study (Figure 7c): $P/P_0 \approx \exp[-(E_D+E_S)/k_BT]$.[16, 25-26] For example, field experiments have suggested $P(\mathrm{He}) > P(\mathrm{Ne}) > P(O_2) > P(\mathrm{Ar}) > P(\mathrm{Kr}) \approx P(\mathrm{Xe}) \approx P(CO_2) \approx P(N_2)$ based on the firn air composition in the bubble close-off zone of polar glaciers.[63-64] Further studies are necessary with well-designed atomistic-level simulations for such molecular gases to precisely understand the gas permeation process, particularly gas *adsorption* on the ice-Ih surface, *penetration* into the ice-Ih lattice structure, and *thermodynamics stability* changes.[16, 25-26, 65] Additionally, considerations should be made on the crystallinity and structural defects in the ice layer surrounding closed-off bubbles. The grain boundaries in a polycrystalline ice and the potential presence of amorphous layer at the gas-ice interface would have effect on both dissolution and molecular diffusion processes.[66-67] The structural and ionic defects in ice-Ih, such as molecular disorientations, ionic defects, and molecular vacancies, might hinder diffusion dynamics (see Refs.[38-39, 68] and other references therein).

Compared to the pristine ice-Ih studied here, its transition to ice clathrate in deeper glaciers would change the diffusion condition for trapped gases.[26, 28] Clathrate hydrates are nonstoichiometric crystals consisting of H_2O-molecular cages in which guest gas molecules (e.g., CO_2 and CH_4) can be trapped.[15, 69-70] This structural difference would lead to remarkably different diffusion dynamics compared to ice-Ih. Although previous studies revealed the diffusion mechanism of CO_2 and CH_4 in clathrate via DFT-based calculations and classical MD simulations, differences in the gas diffusion mechanisms for ice and clathrate have not been systematically investigated.

CONCLUSION

We determined the diffusion paths and electronic diffusion energy barriers (E_D) of noble (He, Ne, Ar, Kr, and Xe) and other major atmospheric gases (CO_2, O_2, and N_2) trapped in ice-Ih. The precise DFT calculations revealed interstitial hopping as the primary diffusion mechanism for both noble and molecular gases investigated here. The noble gases tended to hop along the open hexagonal channel parallel to the *c*-axis, as suggested in previous classical MD simulations. The molecular gases (CO_2, O_2, and N_2) preferred to be aligned parallel to the *c*-axis and, thus, hop along the open hexagonal channel via the interstitial mechanism instead of the previously suggested bond-breaking mechanism. Previously, the bond-breaking mechanism was proposed to explain the faster diffusion of molecular gases than predicted from the potential barriers assuming interstitial hopping. Newly calculated E_D values for CO_2, O_2, and N_2 suggested that fast diffusion of these molecular gases, comparable to those of He and Ne, is possible even via the interstitial mechanism. A direct relationship between E_D and the sizes of hopping gases and the effect of the molecular charge distribution of the hopping gases were established, thereby complementing the experimentally and theoretically determined diffusion trends of gases in ice from an atomistic viewpoint. We believe that a refined understanding of the gas diffusion dynamics in ice can help future paleoclimatic studies to investigate the diffusion-induced elemental and isotopic fractionations in old glacial ice.

Conflict of Interest

The authors declare no conflict of interest.

ACKNOWLEDGEMENTS

This research was supported by research grants (PE21100) from the Korea Polar Research Institute (KOPRI), the National Research Foundation, Korea (NRF-2020R1A3B2079815) to S. K. L., and the supercomputing resources of the KISTI National Supercomputing Center (KSC-2020-CRE0050).

TOC GRAPHICS

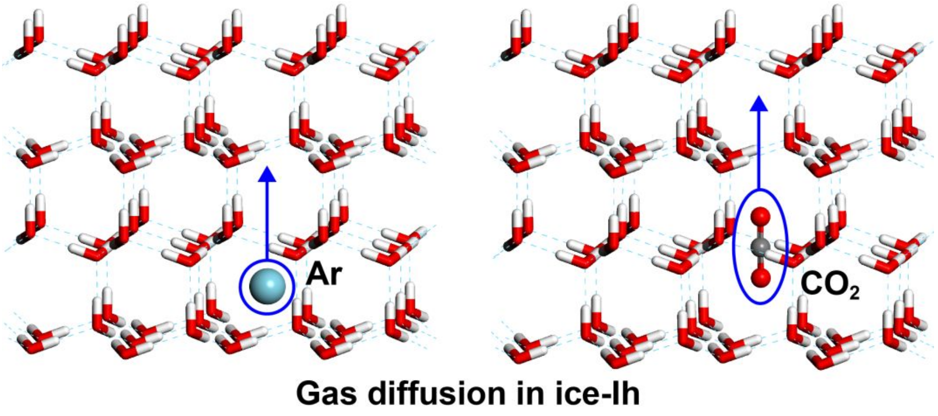

REFERENCES

1. Brook, E. J.; Buizert, C., Antarctic and global climate history viewed from ice cores. *Nature* **2018,** *558* (7709), 200-208.
2. Bender, M.; Sowers, T.; Brook, E., Gases in ice cores. *Proceedings of the National Academy of Sciences* **1997,** *94* (16), 8343-8349.
3. Alley, R. B., Reliability of ice-core science: historical insights. *Journal of Glaciology* **2010,** *56* (200), 1095-1103.
4. Ahn, J.; Headly, M.; Wahlen, M.; Brook, E. J.; Mayewski, P. A.; Taylor, K. C., CO_2 diffusion in polar ice: observations from naturally formed CO_2 spikes in the Siple Dome (Antarctica) ice core. *Journal of Glaciology* **2008,** *54* (187), 685-695.
5. Yan, Y.; Bender, M. L.; Brook, E. J.; Clifford, H. M.; Kemeny, P. C.; Kurbatov, A. V.; Mackay, S.; Mayewski, P. A.; Ng, J.; Severinghaus, J. P.; Higgins, J. A., Two-million-year-old snapshots of atmospheric gases from Antarctic ice. *Nature* **2019,** *574* (7780), 663-666.
6. Stolper, D. A.; Bender, M. L.; Dreyfus, G. B.; Yan, Y.; Higgins, J. A., A Pleistocene ice core record of atmospheric O_2 concentrations. *Science* **2016,** *353* (6306), 1427-1430.
7. Kawamura, K.; Parrenin, F.; Lisiecki, L.; Uemura, R.; Vimeux, F.; Severinghaus, J. P.; Hutterli, M. A.; Nakazawa, T.; Aoki, S.; Jouzel, J.; Raymo, M. E.; Matsumoto, K.; Nakata, H.; Motoyama, H.; Fujita, S.; Goto-Azuma, K.; Fujii, Y.; Watanabe, O., Northern Hemisphere forcing of climatic cycles in Antarctica over the past 360,000 years. *Nature* **2007,** *448* (7156), 912-916.
8. Suwa, M.; Bender, M. L., Chronology of the Vostok ice core constrained by O_2/N_2 ratios of occluded air, and its implication for the Vostok climate records. *Quaternary Science Reviews* **2008,** *27* (11), 1093-1106.
9. Bender, M. L., Orbital tuning chronology for the Vostok climate record supported by trapped gas composition. *Earth and Planetary Science Letters* **2002,** *204* (1), 275-289.
10. Bender, M. L.; Barnett, B.; Dreyfus, G.; Jouzel, J.; Porcelli, D., The contemporary degassing rate of ^{40}Ar from the solid Earth. *Proceedings of the National Academy of Sciences* **2008,** *105* (24), 8232-8237.
11. Buizert, C.; Baggenstos, D.; Jiang, W.; Purtschert, R.; Petrenko, V. V.; Lu, Z.-T.; Müller, P.; Kuhl, T.; Lee, J.; Severinghaus, J. P.; Brook, E. J., Radiometric ^{81}Kr dating identifies 120,000-year-old ice at Taylor Glacier, Antarctica. *Proceedings of the National Academy of Sciences* **2014,** *111* (19), 6876-6881.
12. Adolph, A. C.; Albert, M. R., Gas diffusivity and permeability through the firn column at Summit, Greenland: measurements and comparison to microstructural properties. *The Cryosphere* **2014,** *8* (1), 319-328.
13. Trudinger, C. M.; Enting, I. G.; Etheridge, D. M.; Francey, R. J.; Levchenko, V. A.; Steele, L. P.; Raynaud, D.; Arnaud, L., Modeling air movement and bubble trapping in firn. *Journal of Geophysical Research: Atmospheres* **1997,** *102* (D6), 6747-6763.
14. Schwander, J., Gas Diffusion in Firn. In *Chemical Exchange Between the Atmosphere and Polar Snow*, Wolff, E. W.; Bales, R. C., Eds. Springer Berlin Heidelberg: Berlin, Heidelberg, 1996; pp 527-540.

15. Hassanpouryouzband, A.; Joonaki, E.; Vasheghani Farahani, M.; Takeya, S.; Ruppel, C.; Yang, J.; English, N. J.; Schicks, J. M.; Edlmann, K.; Mehrabian, H.; Aman, Z. M.; Tohidi, B., Gas hydrates in sustainable chemistry. *Chemical Society Reviews* **2020,** *49* (15), 5225-5309.

16. Bereiter, B.; Fischer, H.; Schwander, J.; Stocker, T., Diffusive equilibration of N_2, O_2 and CO_2 mixing ratios in a 1.5-million-years-old ice core. *The Cryosphere* **2014,** *8* (1), 245-256.

17. Satoh, K.; Uchida, T.; Hondoh, T.; Shinji, M. In *Diffusion coefficient and solubility measurements of noble gases in ice crystals*, Proceedings of the NIPR Symposium on Polar Meteorology and Glaciology, Japan, National Institute of Polar Research: Japan, 1995; pp 73-81.

18. Goto, K.; Hondoh, T.; Higashi, A., Determination of diffusion coefficients of self-interstitials in ice with a new method of observing climb of dislocations by X-ray topography. *Japanese journal of applied physics* **1986,** *25* (3), 351-357.

19. Strauss, H. L.; Chen, Z.; Loong, C. K., The diffusion of H_2 in hexagonal ice at low temperatures. *J. Chem. Phys.* **1994,** *101* (8), 7177-7180.

20. Haas, J.; Bullemer, B.; Kahane, A., Diffusion de l'helium dans la glace monocristalline. *Solid State Communications* **1971,** *9* (23), 2033-2035.

21. Metzler, R.; Jeon, J.-H.; Cherstvy, A. G.; Barkai, E., Anomalous diffusion models and their properties: non-stationarity, non-ergodicity, and ageing at the centenary of single particle tracking. *Physical Chemistry Chemical Physics* **2014,** *16* (44), 24128-24164.

22. Higgins, J. A.; Kurbatov, A. V.; Spaulding, N. E.; Brook, E.; Introne, D. S.; Chimiak, L. M.; Yan, Y.; Mayewski, P. A.; Bender, M. L., Atmospheric composition 1 million years ago from blue ice in the Allan Hills, Antarctica. *Proceedings of the National Academy of Sciences* **2015,** *112* (22), 6887-6891.

23. Dahl-Jensen, D., Drilling for the oldest ice. *Nature Geoscience* **2018,** *11* (10), 703-704.

24. Lipenkov, V. Y.; Salamatin, A. N.; Jiang, W.; Ritterbusch, F.; Bender, M. L.; Orsi, A.; Landais, A.; Uchida, T.; Ekaykin, A. A.; Raynaud, D. In *New ice dating tools reveal 1.2 Ma old meteoric ice near the base of the Vostok ice core*, EGU General Assembly 2019, EGU: 2019; pp EGU2019-8505.

25. Maghami, S.; Mehrabani-Zeinabad, A.; Sadeghi, M.; Sánchez-Laínez, J.; Zornoza, B.; Téllez, C.; Coronas, J., Mathematical modeling of temperature and pressure effects on permeability, diffusivity and solubility in polymeric and mixed matrix membranes. *Chem. Eng. Sci.* **2019,** *205* (15), 58-73.

26. Bereiter, B.; Schwander, J.; Lüthi, D.; Stocker, T. F., Change in CO_2 concentration and O_2/N_2 ratio in ice cores due to molecular diffusion. *Geophysical Research Letters* **2009,** *36* (5), L05703.

27. Chepizhko, O.; Peruani, F., Diffusion, Subdiffusion, and Trapping of Active Particles in Heterogeneous Media. *Physical Review Letters* **2013,** *111* (16), 160604.

28. Lüthi, D.; Bereiter, B.; Stauffer, B.; Winkler, R.; Schwander, J.; Kindler, P.; Leuenberger, M.; Kipfstuhl, S.; Capron, E.; Landais, A.; Fischer, H.; Stocker, T. F., CO_2 and O_2/N_2 variations in and just below the bubble–clathrate transformation zone of Antarctic ice cores. *Earth and Planetary Science Letters* **2010,** *297* (1), 226-233.

29. Ikeda-Fukazawa, T.; Kawamura, K.; Hondoh, T., Mechanism of molecular diffusion in ice crystals. *Molecular Simulation* **2004,** *30* (13-15), 973-979.

30. Ikeda-Fukazawa, T.; Kawamura, K.; Hondoh, T., Diffusion of nitrogen gas in ice Ih. *Chemical Physics Letters* **2004,** *385* (5), 467-471.

31. Ikeda-Fukazawa, T.; Horikawa, S.; Hondoh, T.; Kawamura, K., Molecular dynamics studies of molecular diffusion in ice Ih. *J. Chem. Phys.* **2002,** *117* (8), 3886-3896.

32. Kumagai, N.; Kawamura, K.; Yokokawa, T., An interatomic potential model for H_2O: Applications to water and ice polymorphs. *Molecular Simulation* **1994,** *12* (3-6), 177-186.

33. Berendsen, H. J. C., Molecular dynamics simulations: The limits and beyond. In *Computational Molecular Dynamics: Challenges, Methods, Ideas*, Deuflhard, P.; Hermans, J.; Leimkuhler, B.; Mark, A. E.; Reich, S.; Skeel, R. D., Eds. Springer Berlin Heidelberg: Berlin, Heidelberg, 1999; pp 3-36.

34. Silvestrelli, P. L., Hydrogen bonding characterization in water and small molecules. *J. Chem. Phys.* **2017,** *146* (24), 244315.

35. Clark, S. J.; Segall, M. D.; Pickard, C. J.; Hasnip, P. J.; Probert, M. J.; Refson, K.; Payne, M. C., First principles methods using CASTEP. *Z. Kristall.* **2005,** *220* (5-6), 567-570.

36. Gillan, M. J.; Alfè, D.; Michaelides, A., Perspective: How good is DFT for water? *The Journal of Chemical Physics* **2016,** *144* (13), 130901.

37. Goto, A.; Hondoh, T.; Mae, S., The electron density distribution in ice Ih determined by single-crystal x-ray diffractometry. *J. Chem. Phys.* **1990,** *93* (2), 1412-1417.

38. Bartels-Rausch, T.; Bergeron, V.; Cartwright, J. H. E.; Escribano, R.; Finney, J. L.; Grothe, H.; Gutiérrez, P. J.; Haapala, J.; Kuhs, W. F.; Pettersson, J. B. C.; Price, S. D.; Sainz-Díaz, C. I.; Stokes, D. J.; Strazzulla, G.; Thomson, E. S.; Trinks, H.; Uras-Aytemiz, N., Ice structures, patterns, and processes: A view across the icefields. *Rev. Mod. Phys.* **2012,** *84* (2), 885-944.

39. de Koning, M.; Antonelli, A., On the trapping of Bjerrum defects in ice Ih: The case of the molecular vacancy. *J. Phys. Chem. B* **2007,** *111* (43), 12537-12542.

40. Lee, B. H.; Lee, S. K., Effect of lattice topology on the adsorption of benzyl alcohol on kaolinite surfaces: Quantum chemical calculations of geometry optimization, binding energy, and NMR chemical shielding. *Am. Mineral.* **2009,** *94* (10), 1392-1404.

41. Kwon, K. D.; Refson, K.; Sposito, G., Surface complexation of Pb(II) by hexagonal birnessite nanoparticles. *Geochim. Cosmochim. Acta* **2010,** *74* (23), 6731-6740.

42. Kwon, K. D.; Refson, K.; Sposito, G., Zinc surface complexes on birnessite: A density functional theory study. *Geochim. Cosmochim. Acta* **2009,** *73* (5), 1273-1284.

43. Son, S.; Li, W.; Lee, J.-Y.; Kwon, K. D., On the coordination of Mg^{2+} in aragonite: *Ab initio* absorption spectroscopy and isotope fractionation study. *Geochim. Cosmochim. Acta* **2020,** *286* (1), 324-335.

44. Kwon, K. D.; Sposito, G., Dirac's dream: Understanding metal sorption by geomedia using density functional theory. *Chem. Geol.* **2017,** *464* (5), 4-13.

45. Lee, S. K.; Kim, Y.-H.; Yi, Y. S.; Chow, P.; Xiao, Y.; Ji, C.; Shen, G., Oxygen quadclusters in SiO_2 glass above megabar pressures up to 160 GPa revealed by x-ray Raman scattering. *Physical Review Letters* **2019,** *123* (23), 235701.

46. Kim, Y.-H.; Yi, Y. S.; Kim, H.-I.; Chow, P.; Xiao, Y.; Shen, G.; Lee, S. K., Structural transitions in $MgSiO_3$ glasses and melts at the core-mantle boundary observed via inelastic x-ray scattering. *Geophysical Research Letters* **2019,** *46* (23), 13756-13764.

47. Coak, M. J.; Kim, Y.-H.; Yi, Y. S.; Son, S.; Lee, S. K.; Park, J.-G., Electronic and vibrational properties of the two-dimensional Mott insulator $V_{0.9}PS_3$ under pressure. *Phys. Rev. B* **2019,** *100* (3), 035120.

48. Yi, Y. S.; Lee, S. K., Atomistic origins of pressure-induced changes in the O *K*-edge x-ray Raman scattering features of SiO_2 and $MgSiO_3$ polymorphs: Insights from *ab initio* calculations. *Phys. Rev. B* **2016,** *94* (9), 094110.

49. Yi, Y. S.; Lee, S. K., Pressure-induced changes in local electronic structures of SiO_2 and $MgSiO_3$ polymorphs: Insights from *ab initio* calculations of O *K*-edge energy-loss near-edge structure spectroscopy. *Am. Mineral.* **2012,** *97* (5-6), 897-909.

50. Yi, Y. S.; Khim, H.; Kim, Y.-H.; Lee, S. K., Spectral proxies for bonding transitions in SiO_2 and $MgSiO_3$ polymorphs at high pressure up to 270 GPa by O *K*-edge x-ray Raman scattering. *Phys. Rev. B* **2021,** *103* (21), 214109.

51. Parq, J.-H.; Lee, S. K.; Lee, S.-M.; Yu, J., *Ab initio* study of elastic properties of high-pressure polymorphs of CO_2 phases II and V. *J. Phys. Chem. C* **2016,** *120* (40), 23152-23164.

52. Perdew, J. P.; Burke, K.; Ernzerhof, M., Generalized gradient approximation made simple. *Physical Review Letters* **1996,** *77* (18), 3865-3868.

53. Tkatchenko, A.; Scheffler, M., Accurate molecular van der Waals interactions from ground-state electron density and free-atom reference data. *Physical Review Letters* **2009,** *102* (7), 073005.

54. Koelling, D. D.; Harmon, B. N., A technique for relativistic spin-polarised calculations. *Journal of Physics C: Solid State Physics* **1977,** *10* (16), 3107-3114.

55. Barzilai, J.; Borwein, J. M., Two-point step size gradient methods. *IMA J. Numer. Anal.* **1988,** *8* (1), 141-148.

56. Govind, N.; Petersen, M.; Fitzgerald, G.; King-Smith, D.; Andzelm, J., A generalized synchronous transit method for transition state location. *Computational Materials Science* **2003,** *28* (2), 250-258.

57. Friesner, R. A., *Ab initio* quantum chemistry: Methodology and applications. *Proceedings of the National Academy of Sciences of the United States of America* **2005,** *102* (19), 6648.

58. Frish, M.; Trucks, G.; Schiegel, H.; Scuseria, G.; Robb, M.; Cheeseman, J. *Gaussian 09, revision A. 02*, 2009.

59. Koettgen, J.; Zacherle, T.; Grieshammer, S.; Martin, M., *Ab initio* calculation of the attempt frequency of oxygen diffusion in pure and samarium doped ceria. *Physical Chemistry Chemical Physics* **2017,** *19* (15), 9957-9973.

60. Battino, R.; Seybold, P. G., The O_2/N_2 ratio gas solubility mystery. *J. Chem. Eng. Data* **2011,** *56* (12), 5036-5044.

61. Weikusat, I.; Jansen, D.; Binder, T.; Eichler, J.; Faria, S. H.; Wilhelms, F.; Kipfstuhl, S.; Sheldon, S.; Miller, H.; Dahl-Jensen, D.; Kleiner, T., Physical analysis of an Antarctic ice core—towards an integration of micro- and macrodynamics of polar ice. *Philosophical Transactions of the Royal Society A: Mathematical, Physical and Engineering Sciences* **2017,** *375* (2086), 20150347.

62. Karssemeijer, L. J.; de Wijs, G. A.; Cuppen, H. M., Interactions of adsorbed CO_2 on water ice at low temperatures. *Physical Chemistry Chemical Physics* **2014,** *16* (29), 15630-15639.

63. Severinghaus, J. P.; Battle, M. O., Fractionation of gases in polar ice during bubble close-off: New constraints from firn air Ne, Kr and Xe observations. *Earth and Planetary Science Letters* **2006,** *244* (1), 474-500.

64. Huber, C.; Beyerle, U.; Leuenberger, M.; Schwander, J.; Kipfer, R.; Spahni, R.; Severinghaus, J. P.; Weiler, K., Evidence for molecular size dependent gas fractionation in firn air derived from noble gases, oxygen, and nitrogen measurements. *Earth and Planetary Science Letters* **2006,** *243* (1), 61-73.

65. Skyner, R. E.; McDonagh, J. L.; Groom, C. R.; van Mourik, T.; Mitchell, J. B. O., A review of methods for the calculation of solution free energies and the modelling of systems in solution. *Physical Chemistry Chemical Physics* **2015,** *17* (9), 6174-6191.

66. Slater, B.; Michaelides, A., Surface premelting of water ice. *Nat. Rev. Chem.* **2019,** *3* (3), 172-188.

67. Moreira, P. A. F. P.; Veiga, R. G. d. A.; Ribeiro, I. d. A.; Freitas, R.; Helfferich, J.; de Koning, M., Anomalous diffusion of water molecules at grain boundaries in ice Ih. *Physical Chemistry Chemical Physics* **2018,** *20* (20), 13944-13951.

68. Pan, D.; Liu, L. M.; Tribello, G. A.; Slater, B.; Michaelides, A.; Wang, E., Surface energy and surface proton order of ice Ih. *Phys. Rev. Lett.* **2008,** *101* (15), 155703.

69. Buffett, B. A., Clathrate Hydrates. *Annu. Rev. Mar. Science* **2000,** *28* (1), 477-507.

70. Martos-Villa, R.; Mata, M. P.; Sainz-Díaz, C. I., Characterization of CO_2 and mixed methane/CO_2 hydrates intercalated in smectites by means of atomistic calculations. *Journal of Molecular Graphics and Modelling* **2014,** *49*, 80-90.